Nuclear Theory'21
ed. V. Nikolaev, Heron Press, Sofia, 2002

The Electric Form Factor of the Neutron

D. Day

Institute of Nuclear and Particle Physics, Department of Physics, University of Virginia, Charlottesville, VA 22904

Abstract.

The elastic form factors provide valuable information about the charge and magnetization currents inside the proton and neutron. Information on the neutron electric form factor, G_E^n, has proven the most elusive, primarily due to the lack of a free neutron target. The traditional experimental methods used to extract G_E^n are briefly reviewed before discussing the advantages of spin dependent measurements. Details of Jefferson Lab experiment E93026 which measured G_E^n through $\vec{D}(\vec{e}, e'n)p$, will be presented.

1 Introduction

The magnetic moments measurements by Otto Stern in 1934 were the first evidence that the neutron and the proton were composite particles, ones with internal structure. Without compositeness, one would expect the magnetic moment of the proton to be one nuclear magneton and that of the neutron to be zero.

The source of the nucleon anomalous magnetic moments is the strong interaction which gives rise to complex electromagnetic currents of quarks and antiquarks in the nucleon. The non-zero value of the neutron's magnetic moment implies that the neutron must have a charge distribution. Precise knowledge of this charge distribution will give important information about the strong force that binds quarks together in neutrons and protons and other composite particles. The distribution of the charge is contained in an experimentally determined quantity, the electric form factor, G_E^n , a function of momentum transfer.

Nucleons are composed of quarks and gluons and information about their internal structure is critical for testing quark models. For example in a symmetric quark model, with all the valence quarks with the same wavefunction, the charge would everywhere be zero and $G_E^n = 0$. Any deviation from zero exposes the details of the wavefunctions. G_E^n is critical for any study of nuclear structure –

without an accurate description of the nucleon form factors it is almost impossible to obtain information from the few body structure functions, our best testing ground for FSI, MEC, and NN potentials (see, for example, [1]). A precise determination of the charge distribution in the neutron has frustrated physicists for more than 40 years, primarily from the lack of a free neutron target and the fact that the electric form factor is so small. The situation is finally improving because of recent advances in beam and target technology.

2 Nucleon Electromagnetic Form Factors

The diagram in Figure 1 represents the exchange of a virtual photon, carrying energy ν and three momentum $\mathbf{q}$ between the electron and the nucleon target, at rest in the laboratory. The large oval, labeled here as $G_{E,M}$, represents all the information about the structure of the nucleon. In one photon exchange, the elastic scattering of an relativistic electron from a nucleon is described in terms of the Dirac and Pauli form factors, F_1 and F_2 respectively as in,

$$\frac{d\sigma}{d\Omega} = \sigma_{\rm Mott}\frac{E'}{E}\left\{(F_1)^2 + \tau\left[2\left(F_1+F_2\right)^2\tan^2\left(\theta_e/2\right) + (F_2)^2\right]\right\}. \qquad (1)$$

F_1 and F_2 are functions of Q^2 and have the following normalization: $F_1^p(0) = 1$, $F_2^p(0) = 1.79$, $F_1^n(0) = 0$, and $F_2^n(0) = -1.91$. The four momentum transfer $Q^2 = \mathbf{q}^2 - \nu^2 = 4EE'\sin^2(\theta_e/2)$ and $\tau = Q^2/(4M^2)$.

The interpretation of the nucleon form factors has proven more convenient by taking a linear combination of F_1 and F_2, resulting in the *Sachs* electric and

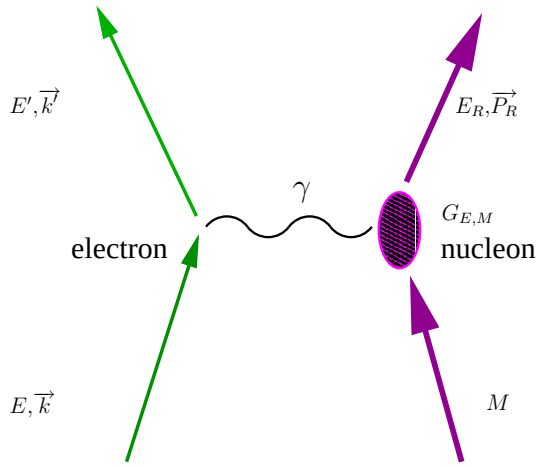

Figure 1. Elastic electron scattering in the one-photon approximation.

magnetic form factors;

$$G_E(Q^2) \equiv F_1(Q^2) - \tau F_2(Q^2), \qquad G_M(Q^2) \equiv F_1(Q^2) + F_2(Q^2). \tag{2}$$

In the $Q^2 = 0$ limit they are given by: $G_E(0) = Q/e$ and $G_M(0) = \mu/\mu_N$, where Q and μ are the charge and the magnetic moment of the nucleon respectively. Specifically, for the proton and neutron:

$$G_E^p(0) = 1, \qquad G_M^p(0) = 2.79, \qquad G_E^n(0) = 0, \qquad G_M^n(0) = -1.91.$$

Making use of the Sachs form factors in Eq. 1 the electron-nucleon cross section expression becomes

$$\frac{d\sigma}{d\Omega} = \frac{\sigma_{Mott}}{(1+\tau)} \frac{E'}{E_0} \left[G_E^2 + \tau(1 + (1+\tau) 2 \tan^2(\theta_e/2)) G_M^2 \right]. \tag{3}$$

This expression is the Rosenbluth formula [2] and unlike Eq. 1 it contains no interference between the electric and magnetic terms. By making measurements at a fixed momentum transfer but different scattering angles the two form factors can, in principle, be separated (via a "Rosenbluth separation").

In the nonrelativistic limit, $Q^2 = \mathbf{q}^{\,2}$, the form factors $G_{E,M}$ can be identified as the Fourier transforms of the symmetric charge and magnetization densities, *e.g.* G_E^n is Fourier transform of the neutron charge distribution $\rho(r)$:

$$\begin{aligned} G_E^n\left(\mathbf{q}^2\right) &= \frac{1}{(2\pi)^3} \int d^3 r \rho(\mathbf{r}) e^{(i\mathbf{q}\cdot\mathbf{r})} \\ &= \int d^3\mathbf{r} \rho\left(\mathbf{r}\right) - \frac{\mathbf{q}^2}{6} \int d^3\mathbf{r} \rho\left(\mathbf{r}\right) \mathbf{r}^2 + \cdots = 0 - \frac{\mathbf{q}^2}{6} \left\langle r_{ne}^2 \right\rangle + \cdots \end{aligned} \tag{4}$$

We can then relate the slope at $Q^2 = 0$ of any the form factors to the mean squared radius of the associated distribution. Specifically, in the case of G_E^n we can relate $\left\langle r_{ne}^2 \right\rangle$ to the decomposition

$$\left\langle r_{ne}^2 \right\rangle = -6 \frac{dG_E^n(0)}{dQ^2} = -6 \frac{dF_1^n(0)}{dQ^2} + \frac{3}{2M_n^2} F_2^n(0) = \left\langle r_{1\mathrm{n}}^2 \right\rangle + \left\langle r_{\mathrm{Foldy}}^2 \right\rangle. \tag{5}$$

The second of these terms, the Foldy term, $\frac{3}{2}\mu_n/M_n^2 = (-0.126)\,\mathrm{fm}^2$, has nothing to do with the rest frame charge distribution while the first is the spatial charge extension seen in F_1^n. $\left\langle r_{ne}^2 \right\rangle$ has been measured [3] through thermal neutron–electron scattering: $\left\langle r_{ne}^2 \right\rangle = -0.113 \pm 0.003 \pm 0.004\,\mathrm{fm}^2$. Consequently $\left\langle r_{1n}^2 \right\rangle = -0.113 + 0.126 \approx 0$. This result suggests that the spatial charge extension seen in F_1^n is about 0 (or very small) and has left the interpretation of G_E^n controversial [4, 5]. This issue now appears to have been resolved [6, 7]

whereby the Foldy term is exactly canceled by a contribution to F_1 that is not related to the charge distribution: G_E^n arises from the rest frame charge distribution of the neutron.

That the neutron have a negative charge radius (and consequently that G_E^n have a positive slope at $Q^2 = 0$) was expected many years ago, given the anomalous magnetic moment of neutron and Yukawa theory of mesons. A negative charge radius can be understood in both a hadronic picture in which there exists a $p\pi^-$ component in the neutron wavefunction that gives rise to a π^- cloud at large radii, and in the constituent quark model in which spin-spin forces between the quarks gives rise to a charge segregation.

2.1 G_E^p and G_M^p Measurements

The electric and magnetic form factors of the proton have been separated via the Rosenbluth technique out to large momentum transfers. The magnetic form factor has been extracted with good precision; however the proton charge form factor data has suffered from the limitations of the Rosenbluth technique at large momentum transfer*. The early form factor data was well described (to the 20% level) by a phenomenological dipole parametrization, where the form factors scaled as

$$G_E^p \quad = \quad G_D = \frac{G_M^p}{\mu_p} = \frac{G_M^n}{\mu_n}, \qquad G_D = \left(1 + \frac{Q^2}{0.71(\mathrm{GeV/c})^2}\right)^{-2}.$$

From Eq. 4 we see that a 'dipole" form factor, $G_D = \left(1 + Q^2/k^2\right)^{-2}$ is generated by an exponential charge distribution: $\rho\left(r\right) \propto e^{-kr}$. In the past, when describing electromagnetic nuclear responses, G_E^n has either been taken to be zero or taken to follow the Galster parametrization [8] of G_E^n from elastic e-D scattering: $G_E^n = -\tau G_D \mu_n/(1 + 5.6\tau)$.

The proton electric and magnetic form factors are shown in Figure 2.

2.2 Neutron Form Factors

The deuteron serves as an approximation of a free neutron target but a firm understanding of the ground and final state wavefunctions is required in order to extract reliable information about the form factors. The lack of a free neutron target and the dominance of G_M^n over G_E^n has, (setting aside recent progress that I will address shortly) left the data set on the neutron form factors much less than desired. The traditional techniques** (restricted to the use of unpolarized beams

*Absolute cross section measurements require precise knowledge of the current and target thicknesses, the solid angles (difficult for magnetic spectrometers), and deadtime and detector efficiencies (when scattering at both forward and backward angles the rates can vary by more than an order of magnitude).

**A nearly complete tabulation of the long history of all the form factor measurements can be found in [10].

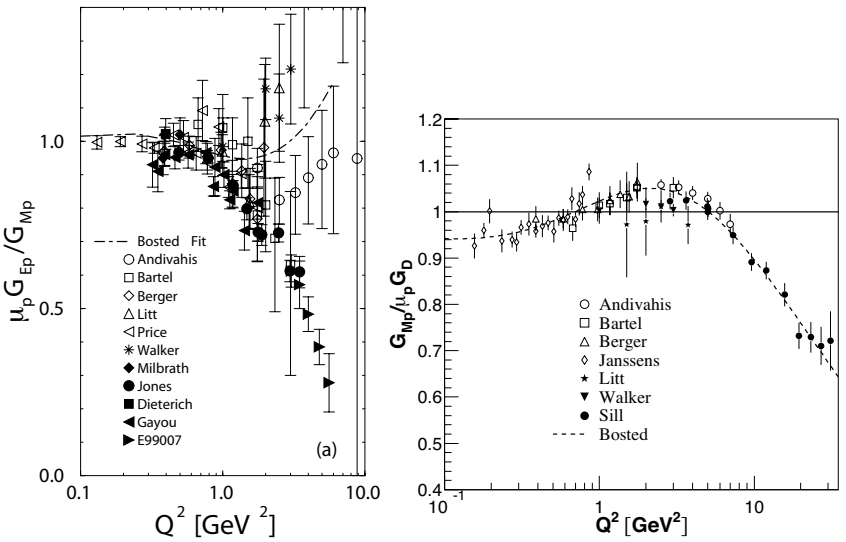

Figure 2. Separated charge and magnetic form factors of the proton from review of [9]. References to the data sets can be found therein.

and targets) used to extract information about G_M^n and G_E^n have been: 1) elastic scattering from the deuteron: $^2\mathrm{H}(e,e')^2\mathrm{H}$, 2) inclusive quasielastic scattering: $^2\mathrm{H}(e,e')X$, 3) scattering from deuteron with the coincident detection of the scattered electron and recoiling neutron: $^2\mathrm{H}(e,e'n)p$, 4) scattering from deuteron with the detection of the scattered electron and the absence of a recoiling proton (anticoincidence) $^2\mathrm{H}(e,e'\bar{\mathrm{p}})\mathrm{p}$, and 5) ratio measurements, $\dfrac{D(e,e'p)}{D(e,e'n)}$, which minimize uncertainties in the deuteron wavefunction and the role of FSI.

Of the techniques enumerated above, 2 and 5 have proven the most successful for G_M^n and 1 and 2 for G_E^n .The systematic differences seen in Figure 3 for G_M^n highlight the limitations of the unpolarized techniques and the pit falls determining the neutron detection efficiency necessary for absolute cross section measurements. A convincing presentation [11] has been made of the consequences to G_M^n if one fails to determine the neutron detection efficiency accurately.

Until the early 1990's the extraction of G_E^n was done most successfully through either small angle elastic electron scattering from the deuteron [8,15–19] or by quasielastic e-D scattering [20–23]. The deuteron is in spin-1 ground state and supports three elastic form factors, G_C , G_Q , G_M. The elastic electron deuteron cross section can be written,

$$\frac{d\sigma}{d\Omega} = \sigma_{NS}\left[A\left(Q^2\right) + B\left(Q^2\right)\tan^2\left(\frac{\theta_e}{2}\right)\right] \tag{6}$$

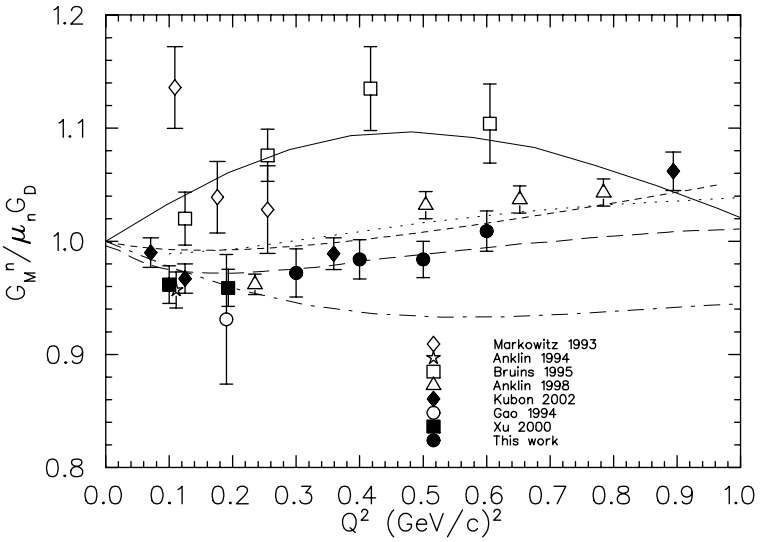

Figure 3. The magnetic form factor of the neutron normalized to the dipole from [14]. Data from points labeled Gao 1994 [12], Xu 2000 [13] and 'this work' [14] are from beam–target asymmetry measurements. References to the other measurements can be found in [14].

where $A(Q^2) = G_c^2 + \frac{8}{9}\eta G_Q^2 + \frac{2}{3}\eta^2 G_M^2$, $B(Q^2) = \frac{4}{3}\eta(\eta+1)G_M^2$, and $\eta = Q^2/(4M_D^2)$. In the Impulse Approximation the elastic cross section is the sum of proton and neutron responses with deuteron wavefunction weighting. In the small θ_e approximation,

$$\frac{d\sigma}{d\Omega} = \cdots (G_E^p + G_E^n)^2 \left[u(r)^2 + w(r)^2\right] j_0(\frac{qr}{2}) dr \cdots \tag{7}$$

As can be see in Eq. 7, the coherent nature of elastic scattering gives rise to an interference term between the neutron and proton response which allows the smaller G_E^n contribution to be extracted. Still, the large proton contribution must be removed. Experiments have been able to achieve small statistical errors but remain very sensitive to deuteron wavefunction model leaving a significant residual dependence on the nucleon–nucleon potential. The most precise data on G_E^n from elastic e-D scattering is shown in Figure 4 from an experiment at Saclay, published in 1990 [19]. The band defined by the various curves is a measure of the theoretical uncertainty ($\approx 50\%$) which can not be avoided.

The published data set on G_E^n has been extended after the realization that the recent high quality data on t_{20} [25] would allow access to G_E^n with smaller theoretical uncertainties than $A(Q^2)$. In the case of $^2\mathrm{H}(e,e')^{2}\overrightarrow{\mathrm{H}}$ components of the

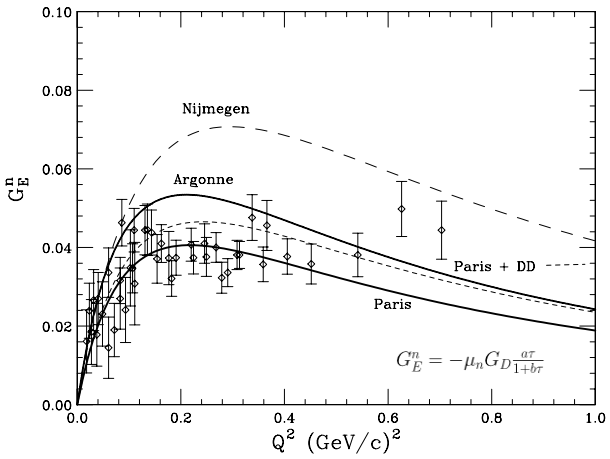

Figure 4. G_E^n from [19]. Plotted with statistical errors are the values of G_E^n extracted from $A(Q^2)$ using the wave function generated with Paris potential. The solid line is a fit to the data using the Galster form shown in the lower right corner. The other lines are similar fits to the data set extracted with Argonne, Nijmegen and the Paris potential with a $\Delta\Delta$ admixture.

tensor polarization give useful combinations of the form factors,

$$t_{20} = \frac{1}{\sqrt{2}S}\left\{\frac{8}{3}\tau_d G_C G_Q + \frac{8}{9}\tau_d^2 G_Q^2 + \frac{1}{3}\tau_d\left[1 + 2(1+\tau_d)\tan^2(\theta/2)\right]G_M^2\right\}.$$

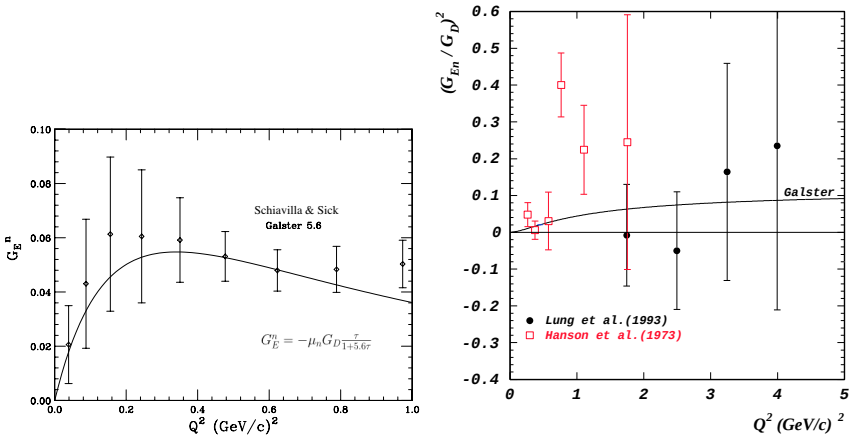

Figure 5. Left: G_E^n extracted from analysis of $^2\mathrm{H}(e,e')^2\vec{\mathrm{H}}$ by [24]. Right: G_E^n at large momentum transfer from quasielastic e-D scattering [23].

By exploiting the fact that $G_Q(Q^2)$ suffers less from theoretical uncertainties than $A(Q^2)$, Schiavilla and Sick [24] were able to extract G_E^n to large momentum transfers. Nonetheless the data set still suffers from large uncertainties - see the left hand panel in Figure 5.

Quasielastic e-D scattering provides a complementary approach to the extraction of G_E^n . In the PWIA model pioneered by Durand and McGee [26, 27] the cross section is incoherent sum of p and n cross section folded with deuteron structure. The extraction of G_E^n requires both a Rosenbluth separation and the subtraction of the sizeable proton contribution. It suffers, unfortunately, from unfavorable error propagation and a sensitivity to the deuteron structure. G_E^n has been extended to $Q^2 = 4$ GeV/c^2 by Lung *et al.* [23] and is reproduced in the right hand side of Figure 5. The large uncertainties allow the data to be consistent with both $G_E^n = 0$ and with $G_E^n =$ Galster. If G_E^n is zero at large Q^2, then F_1^n must cancel τF_2^n (see Eq. 2), begging the question: how does F_1^n evolve from 0 at $Q^2 = 0$ to cancel τF_2^n at large Q^2? However a large F_1^n at large Q^2 is contradicted by data from SLAC experiment E133 [28] which found the ratio of σ_n/σ_p falling with Q^2,. This suggests that $F_1^n \simeq 0$ and G_E^n dominate G_M^n at high Q^2.

2.3 Theory

The nucleon form factors have been described in terms of Vector Meson Dominance (VMD) [29, 30] which constructs the interaction of the photon with the nucleon in terms of the coupling strengths of the virtual photon and the vector mesons and between the vector mesons and the nucleon. Practitioners have adopted various approaches as to which vector mesons to include (all have included the lowest mass mesons, ρ and ω), which of the parameters to be set by data or fit from the nucleon form factors themselves, and to which degree the widths of the mesons are incorporated. The success of these models to describe the form factors at low and moderate Q^2 has been offset by their failure to accommodate the pQCD fall off of the form factors at high Q^2. In quark-dimensional scaling [31] the photon couples to a single quark and each gluon exchange necessary to share the momentum among the quarks contributes a factor proportional to Q^{-2} thereby requiring $F_1 \propto 1/Q^4$ and $F_2 \propto 1/Q^6$. Gari and Krumpelmann incorporated the asymptotic pQCD behavior in a VMD hybrid model [32,33]. In the latter publication the model was modified to include the ϕ meson which has significant consequences for the neutron electric form factor.

There are many models that are based on QCD and for any such model to survive it must predict the nucleon form factors. Attempts to extend pQCD to experimentally accessible values of Q^2 include the work of Kroll *et al.* [34]. The nucleon is manifested in this model as a quark and a diquark with the diquark approximating the role of correlations in the nucleon wave function. Relativistic constituent quark models have been employed to calculate the four nucleon form

factors with a varying degree of success. These include Chung and Coester [35] and Frank, Jennings, and Miller [36]. Other QCD models include the chiral soliton model [37] which describes the basic features of nucleon form factors. It includes relativistic corrections, an extended object (skrymion) and coupling to the vector mesons. The high Q^2 data on G_E^p [54–56] has generated new motivation for the application of these models, see [38]. Dong *et al.* [39] reported a lattice QCD calculation of G_E^n motivated in part by a study of the strangeness magnetic moment of the nucleon. Lu *et al.* [40] has invoked the cloudy bag model to describe the form factors; here the nucleon is expressed as a bag containing three quarks, akin to the MIT bag model, with a pion field coupled to them in such a way that chiral symmetry is respected.

3 Spin Dependent Measurements

It has been known for many years that the nucleon electromagnetic form factors could be measured through spin-dependent elastic scattering from the nucleon [42, 43], accomplished either through a measurement of the scattering asymmetry of polarized electrons from a polarized nucleon target, *e.g.* for the neutron form factors $\vec{D}(\vec{e}, e'n)p$, $^3\vec{\mathrm{He}}(\vec{e}, e'n)pp$, or equivalently by measuring the polarization of the recoiling nucleon, $D(\vec{e}, e'\vec{n})p$ [44]. Since pioneering work on the neutron at Bates [46], the development of high polarization beams and targets, together with high duty factor accelerators, has improved the data set (and outlook) for G_E^n [47–53]. Not incidentally, the recoil polarization technique has allowed precision measurements of G_E^p to nearly 6 GeV/c^2 [54–56].

Asymmetry measurements have significant advantages but they still require the use of a nuclear target in the absence of a free neutron. Coincidence measurements allow one to avoid the subtraction of the dominant proton. Additionally, the difficulties associated with a Rosenbluth separation (absolute cross section measurements) are evaded and the measured asymmetries are much less sensitive to nuclear structure (at least in the case of the deuteron).

The connection between the physics asymmetry and G_E^n can be seen clearly for an (fictitous) vector polarized target of free neutrons with the polarization in the scattering plane and perpendicular to $\vec{q}$. In this case the experimental beam–target asymmetry A_{en}^V [45] can be connected to G_E^n by

$$A_{en}^V = \frac{-2\sqrt{\tau(\tau+1)}\tan(\theta_e/2)G_E^n G_M^n}{(G_E^n)^2 + \tau[1+2(1+\tau)\tan^2(\theta_e/2)](G_M^n)^2}. \tag{8}$$

A_{en}^V is related to the counts asymmetry $\epsilon = (L-R)/(L+R)$, where L, R are charge normalized counts for opposite beam helicities (or target polarizations) by $A_{en}^V = \epsilon/(P_{\mathrm{beam}}P_{\mathrm{neutron}}df)$, where df is the dilution factor due to scattering from materials other than polarized neutrons. Analogous relations exist for recoil

polarization measurements where, in the case of the neutron, the spin component p_x^n substitutes for A_{en}^V.

4 The Electric Form Factor of the Neutron through $\vec{D}(\vec{e}, e'n)p$ at Jefferson Lab

The arrangement of the experiment E93026* which took data at $Q^2 = 0.5$ and $Q^2 = 1.0$ GeV/c^2 in 1998** and 2001 is given in Figure 6. Polarized electrons ($I \leq 100na$) scattered from a polarized target [59] of ^{15}ND$_3$. The polarization axis was oriented in the scattering plane and perpendicular to the central $\vec{q}$. The material was polarized by driving forbidden transitions in the free electron – deuteron system with 140 GHz microwaves. The polarization was measured continuously via NMR.

Electrons were detected in a magnetic spectrometer and a large solid angle array of plastic scintillators provided for both neutron and proton detection. The detector (placed $\approx$ 4m from the target along the direction of $\vec{q}$) consisted of multiple planes of large volume scintillators and included two planes of thin veto paddles and was housed in a large thick walled concrete hut closed on all sides except that facing the target. Each bar and paddle had a phototube at each end to allow good position and timing resolution. The time resolution was determined from the time of flight peak of the gammas (from π^0 decay) in the meantime spectrum and was on the order of 450 ps (σ). In one-photon-exchange the differential coincidence cross section for inelastic polarized electron-polarized deuteron scattering is written as [57]

$$\sigma = \sigma_0(1 + hA_e + P_1^d A_d^V + P_2^d A_d^T + h(P_1^d A_{ed}^V + P_2^d A_{ed}^T)) \qquad (9)$$

where σ_0 is the unpolarized cross section and $A_e, A_d^V, A_d^T, A_{ed}^V, \mathrm{and} A_{ed}^T$ are the electron beam induced asymmetry, the vector and tensor deuteron target asymmetries, and the electron-deuteron vector and tensor asymmetries, respectively. Here P_1^d (P_2^d) is the target vector (tensor) polarization and h is the beam helicity times the electron polarization degree (P_b). A_{ed}^V has been shown to be of special interest [57, 58] when measured in kinematics that emphasize quasi free neutron knockout where it is especially sensitive to G_E^n and relatively insensitive to the nucleon–nucleon (NN) potential describing the ground state of the deuteron, to meson exchange currents (MEC) and to final state interactions (FSI).

*University of Virginia, University of Basel, Florida International University, University of Maryland, Duke University, Hampton University, Jefferson Laboratory, Louisiana Tech University, Mississippi State University, North Carolina A&T St. Univ., Vrije Universiteit, Norfolk State University, Old Dominion University, Ohio University, South. Univ. at New Orleans, Tel Aviv University, Virginia Polytechnic Institute, Yerevan Physics Institute; D. Day, G. Warren, M. Zeier, Spokespersons.

**The data from 1998 at $Q^2 = 0.5$ has been published [53].

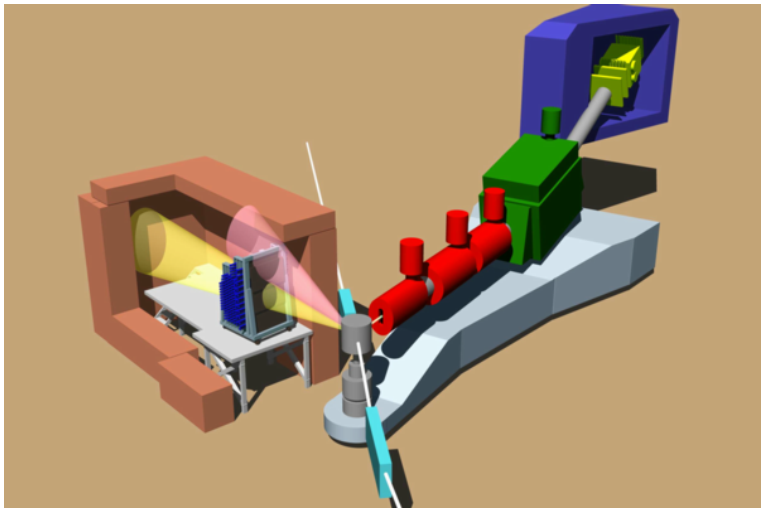

Figure 6. Experimental arrangement in Hall C with cutaway of the neutron detector. The scattered electrons were detected in the HMS (right) and the neutrons and protons were detected in a scintillator array (left). The cones are intended to represent the neutron and protons leaving the target.

The experimental asymmetry*

$$\epsilon = df\frac{P_e A_e + P_e P_t^V A_{ed}^V + P_e P_t^T A_{ed}^T}{1 + P_t^V A_d^V + P_t^T A_d^T} \approx df P_e P_t^V A_{ed}^V \tag{10}$$

arises when the helicity of the beam or the target polarization are reversed. The magnitude of the experimental asymmetry depends on the polarization of the beam and target, and through A_{ed}^V on the kinematics and the orientation of the polarization of the target.

The experimental asymmetry was diluted by scattering from materials other than polarized deuterium nuclei. This includes the nitrogen in $^{15}ND_3$, the liquid helium in which the target was immersed, the NMR coils, and target entrance and exit windows. A Monte Carlo was developed to aid in the determination of the dilution factor and to perform the detector averaging of the theoretical asymmetries and included the neutron detector geometry and approximate efficiencies, the target magnetic field effects on the scattered electrons, the beam raster and radiative effects.

* A_{ed}^T and A_e vanish if symmetrically averaged, A_d^V vanishes with the polarization axis in the scattering plane and A_d^T is suppressed by $P_t^T \approx 3\%$.

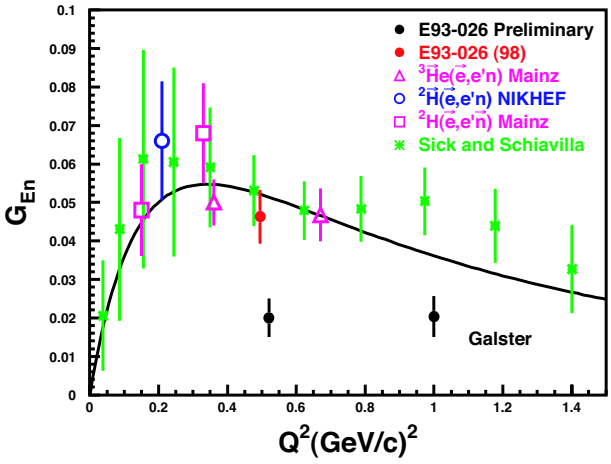

Figure 7. Comparison of present experiment with data from recent spin dependent polarized measurements, [48–52] along with the data set of [24]. The anticipated errors for the 2002 measurement are shown. The solid line is the parametrization ($p = 5.6$) of Galster [8].

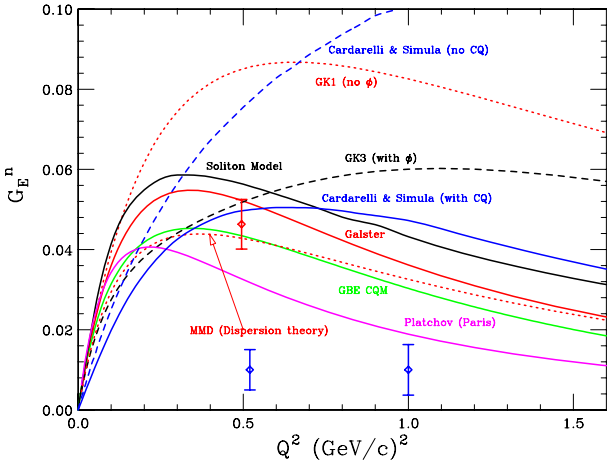

Figure 8. Data from E93026 and various models – the RCQM of [38], soliton model of [37], the Gari-Krumpelmann hybrid VMD model with [33] and without [32] coupling to the ϕ and the dispersion theory of [41].

4.1 Results

In order to extract G_E^n the corrected experimental asymmetry was compared to the Monte Carlo simulation that folds theoretical calculations of the asymmetry with the event distribution across the acceptances of the electron spectrometer and the neutron detector. The theoretical A_{ed}^V values were calculated using the approach of [57,58]. The calculations are based on a non-relativistic description of the $n-p$ system in the deuteron, using the Bonn R-Space NN potential [60] for both the bound state and the description of final state interactions (FSI). The full calculations include also sub-nuclear degrees of freedom such as meson exchange currents (MEC) and isobar configurations (IC) as well as relativistic corrections. The grid of asymmetries was calculated for 3 values of G_E^n given by the Galster parameterization [8] (with $p = 5.6$ and with the magnitude set by an overall scale parameter of 0.5, 1 or 1.5) and the dipole parametrization for G_M^n. The detector averaged theoretical values of A_{ed}^V were obtained for intermediate scale factors by a linear interpolation. The resulting value for G_E^n at $Q^2 = 0.495$ (GeV/c)^2 is $G_E^n = 0.04632 \pm 0.00616 \pm 0.00384$. The 1998 measurement and the projected errors for the 2001 data set (still under analysis) are compared to G_E^n from other polarized experiments [48–52] in Fig. 7. Shown in Fig. 8 are our data compared to some of the available theoretical models.

The outlook for further progress on G_E^n is good. Data at three momentum transfers ($Q^2 = 0.45, 1.1, 1.45$ GeV/c^2) measured via the recoil polarization technique in E93038 [61] at Jefferson Lab are under analysis and a continuation of the Mainz recoil polarization measurements out to $Q^2 = 0.8$ GeV/c^2 is expected to be completed this summer. High precision measurements are expected from the large solid angle detector BLAST at Bates-MIT using polarized internal targets. A new experiment [62] has been approved at Jefferson Lab using a polarized ^{3}He target which will measure G_E^n out to $Q^2 = 3.2$ GeV/c^2. Experiments under analysis, underway, or planned for G_E^n will, in the near future, provide an important test for models of the nucleon and at the same time provide a critical input to our understanding of nuclear structure and dynamics.

References

[1] R.G. Arnold, C. Carlson and F. Gross, (1980) *Phys. Rev.* **C21** 1426.

[2] M. Rosenbluth, (1950) *Phys. Rev.* **79** 615.

[3] S. Kopecki *et al.*, (1995) *Phys. Rev. Lett.* **74** 2427.

[4] Y. A. Alexandrov, (1994) *Neutron News* **5** 20.

[5] J. Byrne, (1994) *Neutron News* **5** 15.

[6] N. Isgur, (1999) *Phys. Rev. Lett.* **83** 272.

[7] M. Bawin and S.A. Coon, (1999) *Phys. Rev.* **C60** 025207.

[8] S. Galster *et al.*, (1971) *Nucl. Phys.* **B32** 221.

[9] E.J. Brash, A. Kozlov, S. Li, and G.M. Huber, (2002) *Phys. Rev.* **C65** 05100.

[10] J.J. Kelly, (1996) in: *Advances in Nuclear Physics*, (eds. J.W. Negele and E. Vogt) **23** pp. 75-294.
[11] J. Jourdan, I. Sick, J. Zhao, (1997) *Phys. Rev. Lett*. **79**, 5186.
[12] H. Gao *et al.*, (1994) *Phys. Rev*. **C50**, R546.
[13] W. Xu *et al.*, (2000) *Phys. Rev. Lett*. **85**, 2900.
[14] W. Xu *et al.*, (2002) arXiv: *nucl-ex/0208007*.
[15] D. J. Drickey and L. N. Hand, (1962) *Phys. Rev. Lett.* **9** 1774.
[16] P. Benaksas *et al.*, (1964) *Phys. Rev. Lett.* **13** 1774.
[17] F.A. Bumiller *et al.*, (1970) *Phys. Rev. Lett.* **25** 1774.
[18] G.G. Simon, *et al.*, (1981) *Nucl. Phys.* **A364** 285.
[19] S. Platchkov *et al.*, (1990) *Nucl. Phys.* **A510** 740.
[20] E.B. Hughes *et al.*, (1965) *Phys. Rev.* **139** B458.
[21] E.B. Hughes *et al.*, (1966) *Phys. Rev* **146** 973.
[22] W. Bartel *et al.*, (1973) *Nucl. Phys.* **B58** 429.
[23] A. Lung *et al.*, (1993) *Phys. Rev. Lett.* **70** 718.
[24] R. Schiavilla and I. Sick, (2001) *Phys. Rev.* **C64** 041002.
[25] D. Abbott *et al.*, (2000) *Phys. Rev. Lett.* **84** 5053.
[26] L. Durand, (1960) *Phys. Rev.* **6** 631.
[27] I.J. McGee, (1967) *Phys. Rev.* **158** 1500; (1967) *Phys. Rev.* **161** 1640.
[28] S. Rock *et al.*, (1992) *Phys. Rev.* **D46** 24.
[29] F. Iachello, A. Jackson and A. Lande, (1973) *Phys. Lett.* **43B** 191.
[30] G. Höhler, *et al.*, (1976) *Nucl. Phys.* **B114** 505.
[31] S. Brodsky and G. Farrar, (1975) *Phys. Rev.* **D11** 1309;
G. Lepage and S. Brodsky, (1980) *Phys. Rev.* **D22** 2157; (1981) *Phys. Scr.* 23 945.
[32] M. Gari and W. Krümpelmann, (1973) *Z. Phys.* **A322** 689; (1986) *Phys. Lett.* **B173** 10.
[33] M. Gari and W. Krümpelmann, (1992) *Phys. Lett.* **B274** 159.
[34] P. Kroll, M. Schurmann, and W. Schweiger, (1992) *Z. Phys.* **A342** 429.
[35] P.L. Chung and F. Coester, (1991) *Phys. Rev.* **D44** 229.
[36] M.R. Frank, B.K. Jennings, and G.A. Miller, (1996) *Phys. Rev.* **C54** 920.
[37] G. Holzwarth, (1996) *Z. Phys.* **A356** 339.
[38] F. Cardarelli and S. Simula, (2000) *Phys. Rev.* **C62** 065201.
[39] S.J. Dong, K.F. Liu, and A.G. Williams, (1998) *Phys. Rev.* **D58** 074504.
[40] D.H. Lu, A.W. Thomas, and A.G. Williams, (1998) *Phys. Rev.* **C57** 2628.
[41] P. Mergell, U.G. Meissner, D. Drechsel, (1996) *Nucl. Phys.* **A596** 367.
[42] A.I. Akhiezer and M.P. Rekalo, (1974) *Sov. J. Part. Nucl.* **3** 277.
[43] N. Dombey, (1969) *Rev. Mod. Phys.* **41** 236.
[44] R.G. Arnold, C. Carlson and F. Gross, (1981) *Phys. Rev.* **C23** 363.
[45] T. W. Donnelly and A. S. Raskin, (1986) *Ann. Phys. (New York)* **169** 247; (1989) **191** 81.

[46] T. Eden *et al;* (1994) *Phys. Rev.* **C50** R1749.

[47] M. Meyerhoff *et al.*, (1994) *Phys. Lett.* **B327** 201.

[48] C. Herberg *et al.*, (1999) *Eur. Phys. J.* **A5** 131.

[49] I. Passchier *et al.*, (1999) *Phys. Rev. Lett.* **82** 4988.

[50] M. Ostrick *et al.*, (1999) *Phys. Rev. Lett.* **83** 276.

[51] J. Becker *et al.*, (1999) *Eur. Phys. J.* **A6** 329.

[52] D. Rohe, *et al.*, (1999) *Phys. Rev. Lett.* **83** 4257.

[53] H. Zhu *et al.*, (2001) *Phys. Rev. Lett.* **87** 081801.

[54] M.K. Jones *et al.*, (2000) *Phys. Rev. Lett.* **84** 1398.

[55] O. Gayou *et al.*, (2001) *Phys. Rev.* **C64** 038292.

[56] O. Gayou *et al.*, (2002) *Phys. Rev. Lett.* **88** 092301.

[57] H. Arenhövel, W. Leidemann and F. L. Tomusiak, (1992) *Phys. Rev.* **C46** 455.

[58] H. Arenhövel, W. Leidemann and F. L. Tomusiak, (1988) *Z. Phys.* **A331** 123.

[59] D. Crabb and D. Day, (1995) *Nucl. Instr and Meth.* **A356** 9; T.D. Averett *et al.*, (1999) *Nucl. Instr. and Meth.* **A427** 440.

[60] R. Machleidt, K. Holinder and Ch. Elster, (1987) *Phys. Rep.* **149** 1.

[61] B.D. Anderson, S. Kowalski and R. Madey, (1993) *Jefferson Lab experiment E93038.*

[62] B. Wojtsekhowski *et al., Jefferson Lab proposal E02-013*.